Stress versus strain controlled shear: Yielding and relaxation of concentrated colloidal suspensions

A. Pamvouxoglou, A. B. Schofield, G. Petekidis, S. U. Egelhaaf, et al.

Citation: Journal of Rheology **65**, 1219 (2021); doi: 10.1122/8.0000212
View online: https://doi.org/10.1122/8.0000212
View Table of Contents: https://sor.scitation.org/toc/jor/65/6
Published by the The Society of Rheology

Stress versus strain controlled shear: Yielding and relaxation of concentrated colloidal suspensions

A. Pamvouxoglou,[1,a)] A. B. Schofield,[2] G. Petekidis,[3] and S. U. Egelhaaf[1,b)]

[1]*Condensed Matter Physics Laboratory, Heinrich Heine University, 40225 Düsseldorf, Germany*
[2]*School of Physics and Astronomy, The University of Edinburgh, Edinburg EH9 3FD, Scotland, United Kingdom*
[3]*IESL-FORTH and Materials Science and Technology Department, University of Crete, 71110 Heraklion, Greece*

(Received 20 December 2020; final revision received 29 July 2021; published 13 September 2021)

Abstract

In rheological experiments, the relationship between stress and strain is determined. In the transient regime, this relationship may depend on which of these properties is applied and which is measured. In general, data collected using one or the other as the control parameter are not necessarily equivalent. Moreover, the assumed steady state and the relaxation following this state might depend on whether stress or strain has been applied. We examined colloidal suspensions with concentrations around the glass transition and compared their response to stress and strain, in particular, their transient response after the start-up of shear, their steady state, and their relaxation after cessation of shear. After the start-up of shear, the transient behavior was found to significantly depend on whether the sample is exposed to a constant shear rate or a constant stress. Nevertheless, the transients lead to a rheological steady state that is independent of how it is reached, as long as yielding occurred and the corresponding shear rate or stress is applied. After cessation of shear, the relaxation under strain and stress control shows both similarities and differences. This is quantified based on, e.g., the hydrodynamic, Brownian, and residual stress as well as the recovered strain. In addition, the responses of the rheometers to the abrupt changes have been characterized. The corresponding technical data are presented and taken into account in the data interpretation. https://doi.org/10.1122/8.0000212

I. INTRODUCTION

The dynamics of concentrated colloidal suspensions is dominated by crowding [1–3]. Around each particle, the neighboring particles form a "cage" and are themselves caged by their neighbors. Particles tend to remain in their cages and hence their motions are restricted, typically to about a tenth of their size. Out-of-cage motions are severely limited and long-time diffusion is suppressed. As the volume fraction is increased, the particle motion is increasingly restricted and arrested beyond the glass transition [3–5]. As a consequence, the system becomes trapped in a non-equilibrium state whose properties depend on the sample history.

Upon external driving, the particle dynamics competes with the imposed time scale. The slow particle dynamics is reflected in, e.g., the rheological properties [6–24]. Small deformations or stresses lead to an essentially elastic response and the system behaves as a viscoelastic solid [20–23,25,26]. However, the application of a large strain rate or a large stress can yield the sample and, beyond the yield point, induce steady flow [19–21,27–36]. Then, the viscous behavior dominates the elastic behavior and the response of the sample becomes fluid-like [19–21,37].

The transition from the solid-like to the fluid-like behavior is characterized by transient phenomena [35–40]. At rest, the behavior is dominated by cages that are, on average, isotropic. Upon the application of a constant shear rate, the local microscopic structure becomes anisotropic. The cage deformations release some of the restrictions and cause the sample to yield. The deformations increase to a maximum that coincides with a maximum in the measured stress. Subsequently, the deformations and stored stresses are partially relaxed and the measured stress decreases toward a plateau that indicates a steady state. In the steady state, cages continuously break and reform and fluid-like behavior is observed [40–42]. Similarly, the application of a constant shear stress also leads to fluidization but only if the applied stress is larger than the yield stress [19–21,33,34,43]. For stresses below the yield stress, the system does not show steady-state flow but creep with the strain increasing sublinearly with time [33,34,43–47].

This implies that the transient and yielding behavior is different depending on whether the experiment is strain or stress controlled [38]. Moreover, the steady state identified by its rheological properties might not be unique with respect to the microscopic state, i.e., the arrangement and dynamics of the particles. Thus, the relaxation following the cessation of shear might depend on sample history. The application of a constant shear rate eventually causes yielding, whereas yielding can be avoided under constant stress if the applied stress is below the yield stress. Hence, qualitatively different behaviors are observed in otherwise analogous rheological protocols. Furthermore, the relationship between the rheological response and the microscopic particle dynamics depends on whether strain or stress is applied. The strain is linearly related to the mean squared displacement (MSD) if a constant stress is applied [43], whereas no linear relation between strain and MSD is found in strain-controlled experiments [35,39,40].

[a)]Electronic mail: Andreas.Pamvouxoglou@uni-duesseldorf.de
[b)]Author to whom correspondence should be addressed; electronic mail: Stefan.Egelhaaf@uni-duesseldorf.de

In the glass state, the dynamics is arrested and the system trapped in a non-equilibrium state. The sample history hence is important. Therefore, the rheological protocol and, in general, the sample preparation and treatment become crucial. This has important consequences. For example, special care is required to reproducibly prepare, load, or rejuvenate a sample. It also offers the opportunity to control the properties and behavior of materials without changing their composition [48].

In this paper, the rheological responses to stress- and strain-controlled shear are compared using a simple model system that can become trapped in a non-equilibrium state and hence shows history-dependent properties. We investigated the behavior of colloidal suspensions of poly(methyl methacrylate) (PMMA) spheres, which show hard-sphere-like behavior [49] and have been studied extensively [19,22,23,26,27,36,37,39–41,43,50]. Three concentrated samples were examined with volume fractions below, just above, and well above the glass transition. Their transient behavior and the steady state were investigated by applying either a constant shear rate or a constant stress (Fig. 1, left). Relaxation experiments were performed with the shear rate or the stress fixed to zero (Fig. 1, right). Both these tests were performed regardless of whether a constant shear rate or a constant stress had initially been applied to the system. Therefore, the effect of the concurrent as well as previous treatments and hence the different effects of stress or strain as well as the different sample histories can be investigated. We found that the transient behavior after start-up of shear heavily depended on whether a constant shear rate or a constant stress was applied. In contrast, once the rheological steady state had been achieved, it was found that its mechanical properties do not depend on the type of experiment, i.e., the application of strain or stress, as long as yielding had occurred. Finally, the different relaxations follow a similar although not necessarily an identical evolution, depending on both the conditions imposed during shear and those applied after its cessation.

II. MATERIALS AND METHODS

A. Sample preparation

The samples contained PMMA spheres (density $1.18\,\mathrm{g/cm^3}$) stabilized with poly(12-hydroxy-stearic acid) (PHSA, density $0.9\,\mathrm{g/cm^3}$). Their radius was determined to be $R = 157$ nm (by static light scattering) and their polydispersity to be approximately 25% with a moderate positive skewness of 0.72 and a kurtosis of 3.1 (as determined by scanning electron microscopy), which is close to the kurtosis of a Gaussian distribution. The particles were dispersed in squalene (TCI, CAS 111-02-4, density $0.92\,\mathrm{g/cm^3}$) which has a refractive index ($n_s = 1.499$) similar to that of PMMA ($n_p \approx 1.497$) as well as a very high boiling point (458 °C), which meant that evaporation was negligible during the rheological experiments.

Centrifugation at about 3500g resulted in a random close packed (RCP) suspension, which was used as stock suspension. Samples with different volume fractions ϕ were prepared

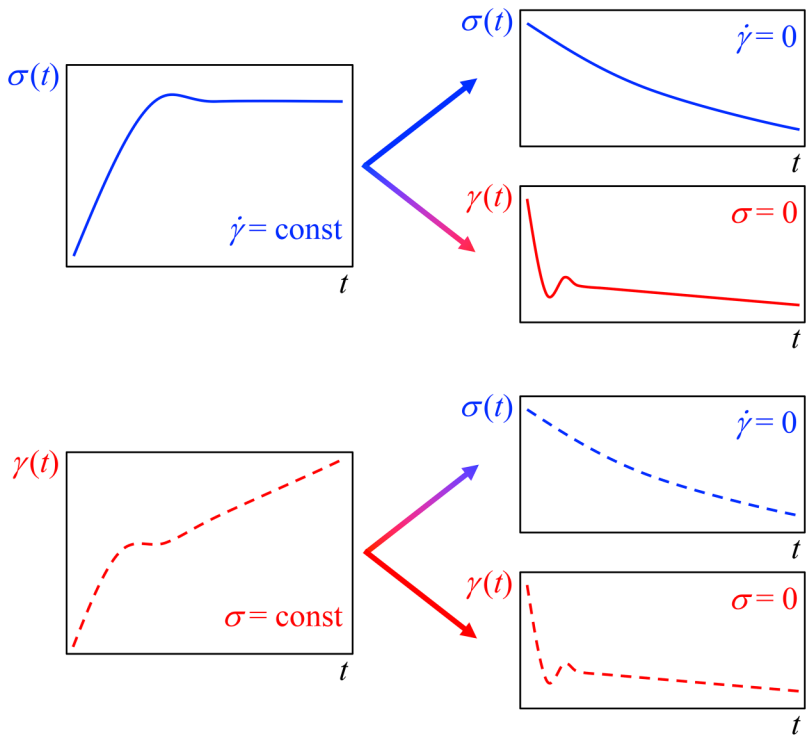

FIG. 1. Schematic representation of the performed tests. (Left) Initially, the response after start-up shear was investigated. Either a constant shear rate $\dot{\gamma}$ was applied and the stress σ measured (top) or a constant stress σ was applied and the strain γ measured (bottom). (Right) After the cessation of shear, the relaxation was followed. Usually, after the application of a constant shear rate, the shear rate is set to zero, $\dot{\gamma} = 0$, and the stress relaxation $\sigma(t)$ determined (top) or after the application of a constant stress, the stress is set to zero, $\sigma = 0$, and the strain relaxation $\gamma(t)$ determined (bottom). We also studied the unconventional combinations that involve a change of the control parameter. After the application of a constant shear rate $\dot{\gamma}$, the stress was set to zero, $\sigma = 0$, and the strain relaxation $\gamma(t)$ determined or after the application of a constant stress σ, the strain rate was set to zero, $\dot{\gamma} = 0$, and the stress relaxation $\sigma(t)$ determined (two panels in the middle).

by direct dilutions of the stock suspension. Their normalized elastic modulus, $G'R^3/k_BT$, where k_BT is the thermal energy, was determined and compared to previously reported values (Appendix A) [36,51]. This indicates consistent volume fractions of the samples, $\phi = 0.575$, 0.602, and 0.624. Furthermore, this implies a volume fraction of the stock suspension $\phi \approx 0.67$, which is close to literature values for a RCP suspension [52–54] and hence consistent within the expected uncertainty of the volume fraction [55].

For the investigated particles, the Brownian time $\tau_{B,0} = R^2/D_0 = 0.22$ s with the diffusion coefficient of individual particles, $D_0 = k_BT/(6\pi\eta R) = 0.11\,\mu m^2/s$, and the viscosity of squalene, $\eta = 12$ cP. The effect of interactions is taken into account by considering $\tau_{B,\phi} = R^2/D(\phi)$ with the ratio $D(\phi)/D_0$ taken from the literature [3] and resulting in $\tau_{B,\phi} = 1.86$ s, 2.41, and 3.17 s for $\phi = 0.575$, 0.602, and 0.624, respectively.

B. Rheological measurements

The measurements were performed with three different rheometers to optimize the conditions for strain or stress control and for the required time response. First, a fast strain-controlled rheometer with a separate motor and transducer (ARES G2, TA Instruments) with a cone-plate geometry with a diameter $d = 25$ mm and cone angle $\theta = 2°$ was used to perform step-rate experiments with $\dot{\gamma} \geq 0.5\,s^{-1}$ that required a fast instrument response and data acquisition. Second, a stress-controlled rheometer with a combined motor and transducer but also an appropriate strain control mode based on an embedded feedback-loop (MCR-302 WESP, Anton Paar) with a cone-plate geometry with $d = 25$ mm and $\theta = 1.57°$ was applied for step rate and creep experiments. Third, a stress-controlled rheometer with a combined motor and transducer (AR2000EX, TA Instruments) with a cone-plate geometry with $d = 25$ mm and $\theta = 2°$ was used for creep experiments. A detailed attribution of the rheometers to the different tests as well as a description of the response of the rheometers after commanding them to apply the desired shear is very briefly given in Appendix B and detailed in the supplementary material [56] where the response resulting from the interplay of the rheometer, geometry, and sample are quantified for the different instruments and conditions. To avoid slip, all cones and plates were serrated with a roughness of about 10 μm. Although a solvent with a high boiling point was chosen, evaporation was further reduced using a home-built solvent trap ensuring that evaporation is insignificant during the measurements. This allowed for experiments lasting up to 7 days. All measurements were performed at 20 °C.

Before each experiment, a rejuvenation protocol was performed to reduce history, especially loading, effects and improve the reproducibility. The rejuvenation protocol consisted of oscillatory shear with an angular frequency $\omega = 1$ rad/s and a strain amplitude decreasing from $\gamma = 1000\%$ to $\gamma = 0.1\%$. Subsequently, a period of zero stress, $\sigma = 0$ Pa, was applied for 200 s during which the recovered strain dropped to a value within the linear regime (Fig. 11) and hence deformations, including anisotropic deformations, are minimized. Between individual measurements, dynamic frequency sweeps (DFS) were performed to check for aging effects. The DFS results do not indicate any significant change in the rheological properties during the experiments. This suggests that aging was not significant and an initial state with reproducible rheological properties was obtained by the applied rejuvenation protocol.

III. RESULTS AND DISCUSSION

A. Strain-controlled experiments: Step rate and relaxation

1. Step-rate experiments

In a step-rate experiment, a constant shear rate $\dot{\gamma}$ is applied to the initially quiescent, solid-like sample until a steady state with a fluid-like flow is reached. (For the response of the rheometer after commanding it to apply a constant shear rate, see Appendix B and, in particular, the supplementary material [56].) During the experiment, the stress response of the sample, $\sigma(t)$, is monitored with the time linearly related to the strain, $t = \gamma/\dot{\gamma}$. Figures 2(A)–2(C) present the stress evolution $\sigma(\gamma)$ of the samples subjected to different applied shear rates $\dot{\gamma}$, where only data that are measured after the set shear rate $\dot{\gamma}$ has been reached are shown.

The linear increase in the stress $\sigma(\gamma)$ at small strains γ indicates solid-like behavior. However, already at deformations $\gamma < 0.1$ deviations from a linear dependence are noticeable and indicate viscous contributions to the mainly solid-like response [37]. Subsequently, a maximum in the stress $\sigma(\gamma)$ is reached, the stress overshoot. The overshoot moves to higher strains and first becomes more and then less pronounced as the shear rate $\dot{\gamma}$ increases, as was reported previously [36,37,40,42]. With increasing volume fraction, the overshoot becomes less pronounced because the increasingly dense packing restricts cage deformations. Beyond the overshoot, stress is released. Hence, the stress decreases to reach a plateau value, the steady-state stress σ_{ss}. The steady-state stress σ_{ss} increases with increasing shear rate $\dot{\gamma}$ and increasing volume fraction ϕ [Figs. 2(A)–2(C)], in agreement with other studies [36,37,40,42]. The dependence of σ_{ss} on the shear rate $\dot{\gamma}$ can be compared with the flow curve, which will be discussed in Sec. III C 1.

2. Relaxation experiments

After a steady state was reached, shear was stopped by imposing $\dot{\gamma} = 0$ rad/s (Appendix B and the supplementary material [56], especially Fig. S3) and the stress relaxation $\sigma(t)$ was followed [Figs. 2(D)–2(F)]. The stress $\sigma(t)$ shows a fast, on the time scale of the experiments instantaneous, initial relaxation followed by a slow, in the experiments observable, relaxation as well as some residual stress. As will be explained below, the fast initial relaxation is attributed to the hydrodynamic stress and the slow relaxation to the Brownian stress. In addition, contact (or friction) forces might occur, which can be determined in shear reversal experiments [57,58]. We assume that contact forces are negligible because shear-thickening does not occur.

The initial fast decay is related to the relaxation of the suspending liquid which relaxes much faster than the particles.

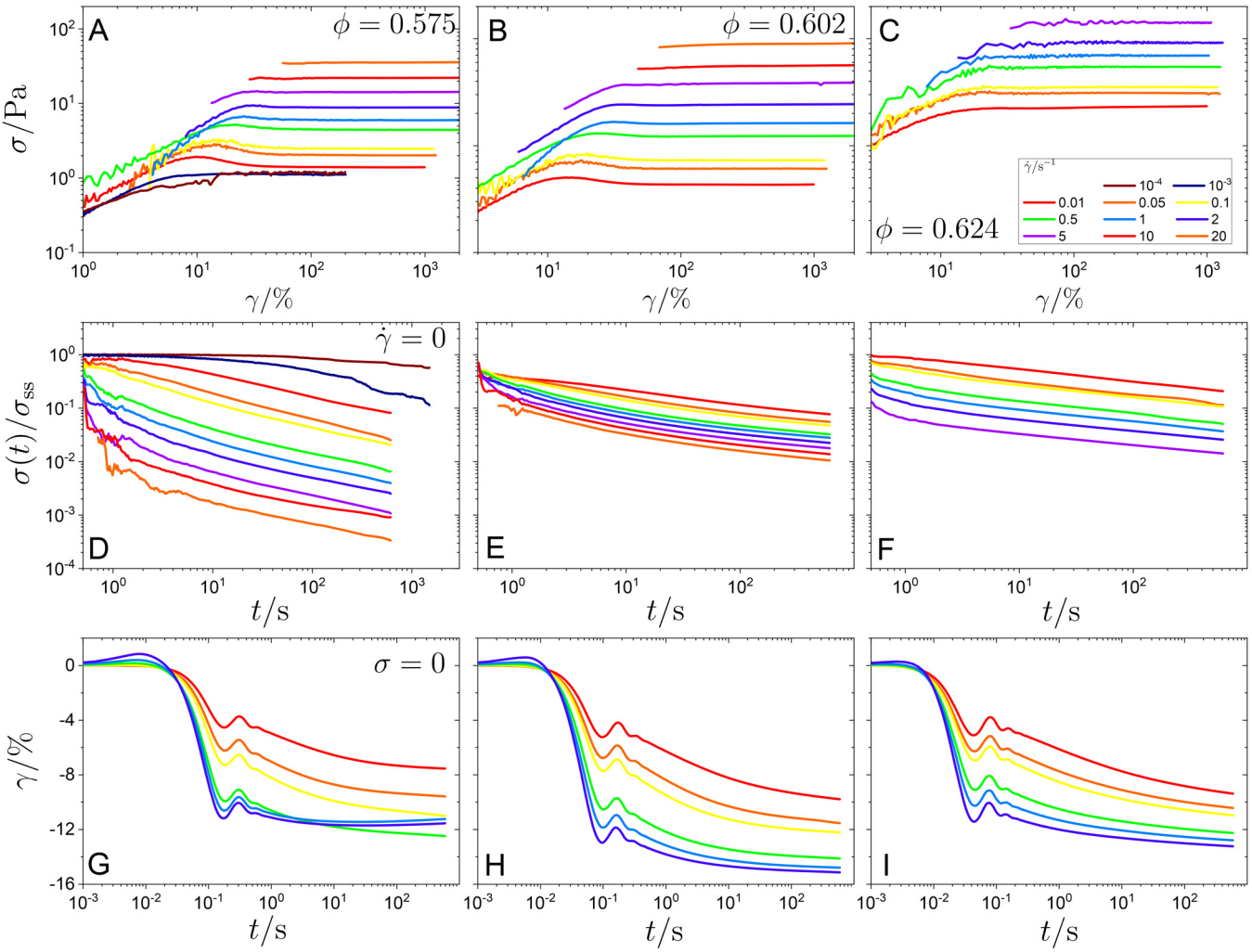

FIG. 2. (A)–(C) Step-rate measurements with constant applied shear rate $\dot{\gamma}$ (as indicated). Measured stress σ as a function of strain $\gamma = \dot{\gamma}t$, which corresponds to the temporal evolution. (D)–(F) Stress relaxation $\sigma(t)$ normalized by the steady-state stress σ_{ss} after the shear rate [as in (A)–(C)] has been stopped and fixed to $\dot{\gamma} = 0\,\mathrm{s}^{-1}$. (G)–(I) Strain relaxation $\gamma(t)$ after the shear rate [as in (A)–(C)] has been stopped and the stress fixed to $\sigma = 0\,\mathrm{Pa}$. Volume fractions ϕ are [(A), (D), and (G)] 0.575, [(B), (E), and (H)] 0.602, and [(C), (F), and (I)] 0.624.

This part of the relaxed stress is accordingly considered the hydrodynamic stress σ_h. Previously, the hydrodynamic stress has been determined in computer simulations [57,59]. In shear thickening suspensions, furthermore, shear reversal in oscillatory shear experiments as well as shear cessation experiments revealed its dependence on the shear rate [58,60,61]. Due to its fast decay, the relaxation of the hydrodynamic stress cannot be monitored in a shear cessation test but its magnitude can be determined from the initial stress drop. The hydrodynamic stress σ_h [Fig. 3(A), filled triangles] is identified with the decay of $\sigma(t)$ to the first reliable data point [Figs. 2(D)–2(F)]. For the two lowest shear rates, the magnitude of the hydrodynamic stress is very small, similar to the uncertainty of the measurement. (The data corresponding to the two lowest shear rates $\dot{\gamma} = 10^{-4}\,\mathrm{s}^{-1}$ and $10^{-3}\,\mathrm{s}^{-1}$ are not included in Fig. 3.) At intermediate and high shear rates $\dot{\gamma}$, the hydrodynamic stress closely approaches the steady-state stress σ_{ss} [Fig. 3(D), filled triangles] and hence represents the major part of the relaxation. It increases approximately linearly with shear rate $\dot{\gamma}$ [Fig. 3(A)], in agreement with previous experimental and simulational studies [57–60]. The hydrodynamic stress normalized by the steady-state stress, σ_h/σ_{ss}, shows no significant dependence on the volume fraction ϕ. The hydrodynamic stress furthermore displays a similar dependence on the volume fraction ϕ as the yield stress $\sigma_{y,DSS}$ [Fig. 3(A), horizontal dashed lines; for values, see Table I in Appendix A]. Hence, $\sigma_h/\sigma_{y,DSS}$ also shows no significant dependence on the volume fraction ϕ (data not shown).

The slow decay that occurs after the first reliable data point is due to the Brownian stress σ_B [58]. It is attributed to the relaxation of the shear-induced anisotropic arrangement of particles. This slow relaxation occurs on short length scales in the near-contact boundary layer as well as on larger length scales corresponding to rearrangements of the anisotropic cage [57]. These two length scales are reflected in two time scales that govern the decay of the Brownian stress [Figs. 2(D)–2(F)]. The rapid portion is particularly pronounced for large initially applied shear rates that did not allow for short-ranged cage rearrangements and hence these rearrangements occur during the relaxation. The Brownian stress decreases only moderately with increasing

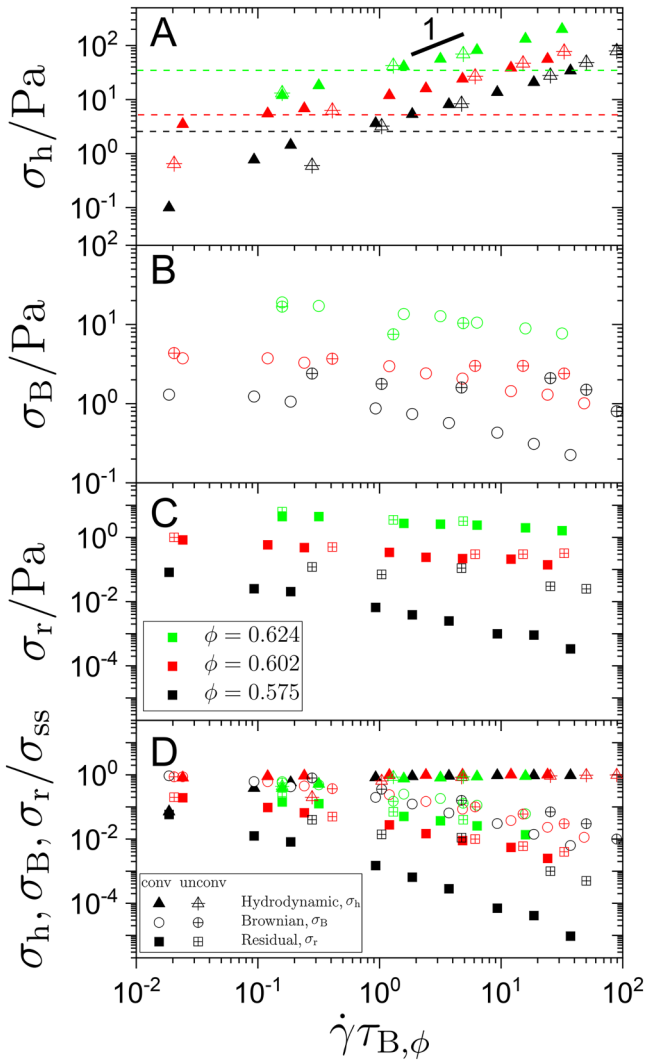

FIG. 3. Components of the stress relaxation: (A) hydrodynamic σ_h, (B) Brownian σ_B, and (C) residual stress σ_r as a function of the shear rate $\dot{\gamma}$ normalized by the Brownian time $\tau_{B,\phi}$. (D) Same stresses but normalized by the steady-state stress σ_{ss}. Data were obtained in conventional experiments [Figs. 2(D)–2(F)], i.e., the application of a constant shear rate $\dot{\gamma}$ was followed by relaxation while $\dot{\gamma} = 0\,\mathrm{s}^{-1}$, and unconventional experiments [Figs. 4(G)–4(I)], i.e., the application of a constant stress σ was followed by relaxation while $\dot{\gamma} = 0\,\mathrm{s}^{-1}$ (symbols as indicated). The yield stresses $\sigma_{y,DSS}$ are indicated as horizontal dashed lines in (A). Volume fractions ϕ as indicated.

shear rate $\dot{\gamma}$ [Fig. 3(B), open circles]. An almost constant Brownian stress is consistent with a decreasing Brownian contribution to the viscosity, as observed by Stokesian dynamics, and an increasing shear rate $\dot{\gamma}$ [57,59]. However, the Brownian stress normalized by the steady-state stress, σ_B/σ_{ss}, decreases with increasing previously applied shear rate $\dot{\gamma}$ and is almost independent of volume fraction ϕ [Fig. 3(D), open circles]. At the smallest previously applied shear rates, individual sudden drops are observed which are attributed to avalanche type cooperative particle rearrangements [33,62]. At small previously applied shear rates, the contribution of the Brownian stress is similar to the hydrodynamic stress whereas at large shear rates the contribution of the Brownian stress becomes insignificant and the hydrodynamic stress dominates (irrespective of whether the absolute values or the values normalized by the steady-state stress or yield stress are considered). The transition occurs at $\dot{\gamma}\tau_{B,\phi} \approx 1$, where $\tau_{B,\phi}$ is the Brownian time taking into account interactions (Sec. II A).

The very slow dynamics with suppressed out-of-cage motions prevents a complete relaxation of the shear-induced anisotropic arrangement of the particles even at the longest times investigated. Hence, a residual stress σ_r remains, as previously reported [18,63–67]. This reflects some remaining solid-like character, which becomes less pronounced as the sample is more thoroughly fluidized at larger shear rates $\dot{\gamma}$. Correspondingly, the residual stress σ_r and the normalized residual stress, σ_r/σ_{ss} or $\sigma_r/\sigma_{y,DSS}$, decrease with increasing shear rate $\dot{\gamma}$ [Figs. 3(C) and 3(D), filled squares]. The decrease of σ_r is very small for the largest volume fraction $\phi = 0.624$. There is a significant ϕ dependence of the residual stress σ_r and of the normalized residual stress σ_r/σ_{ss} or $\sigma_r/\sigma_{y,DSS}$.

B. Stress-controlled experiments: Step-stress and recovery

1. Step-stress (creep) experiments

In a creep experiment, a constant stress σ is applied and the resulting deformation $\gamma(t)$ measured as a function of time t. The response $\gamma(t)$ is qualitatively different depending on whether the applied stress σ is below or above the yield stress σ_y (Table I in Appendix A). For large applied stresses $\sigma > \sigma_{y,DSS}$, the increase of $\gamma(t)$ is super-linear initially and linear at later times [Figs. 4(A)–4(C)]. A slope of one implies a constant shear rate $\dot{\gamma}$ and hence a constant viscosity $\eta = \sigma/\dot{\gamma}$. This indicates that the system flows and hence has yielded. It has reached a steady state and the stress σ and shear rate $\dot{\gamma}$ can be compared to the flow curve (Sec. III C 1). If $\sigma < \sigma_{y,DSS}$, initially $\gamma(t)$ also increases superlinearly but then hardly increases at long times. This sublinear increase of $\gamma(t)$ is related to Andrade creep and has also been observed for other yield stress materials [33,47,68]. Even at very long times, $t \approx 10^5$ s, the slope keeps increasing but remains significantly lower than one (data not shown), as previously observed [33]. This indicates that the sample did not flow and hence did not yield. Accordingly, no steady state is reached and hence the stress σ and shear rate $\dot{\gamma}$ do not correspond to any point on the flow curve (Sec. III C 1). Only if the applied stress is close to the yield stress, $\sigma \lesssim \sigma_{y,DSS}$, at long times an approximately linear increase and hence a steady state with a constant shear rate might be observed indicating yielding and flow.

Between the short and long-time regimes, at $t \approx 0.5$ s, oscillations are observed [Figs. 4(A)–4(C)]. Similar oscillations have previously been reported and related to the interplay between instrument inertia, sample elasticity, and shear wave propagation [33,38,43,68,74–76]. The oscillations are prominent for stresses $\sigma \lesssim \sigma_{y,DSS}$ where the sample elasticity and inertia effects have a similar magnitude. At stresses $\sigma \gtrsim \sigma_{y,DSS}$, the sample is fluidized and oscillations are considerably less pronounced and, for $\sigma \gg \sigma_{y,DSS}$, oscillations are no longer observed.

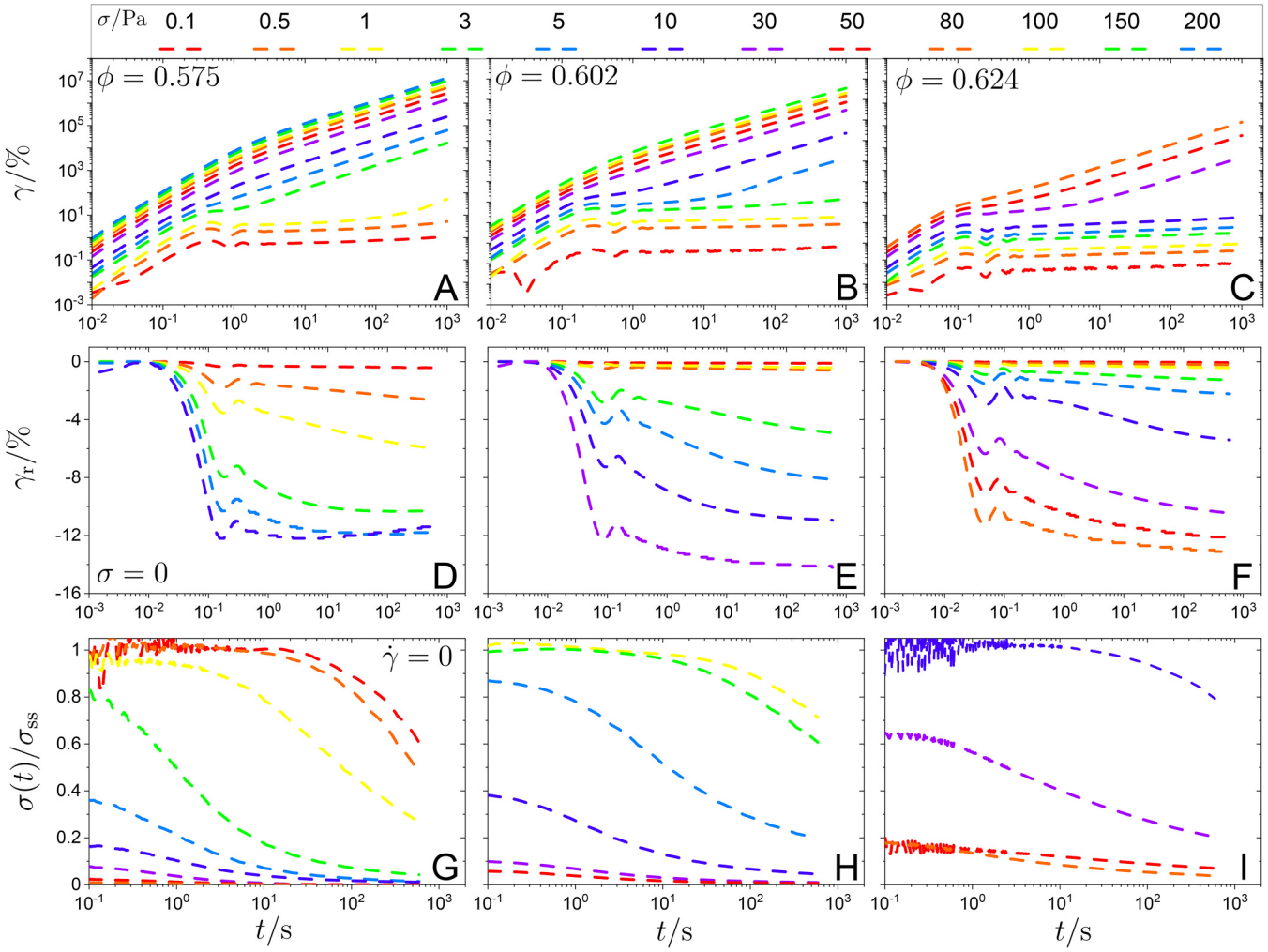

FIG. 4. (A)–(C) Creep measurements with constant applied stress σ (as indicated). Measured strain $\gamma(t)$ as a function of time t. (D)–(F) Recovered strain $\gamma_r(t)$ after the stress [as in (A)–(C)] has been released and fixed to $\sigma = 0$ Pa. (G)–(I) Stress relaxation $\sigma(t)$ normalized by the steady-state stress σ_{ss} after the stress [as in (A)–(C)] has been released and the shear rate fixed to $\dot{\gamma} = 0\,s^{-1}$. The data at short times in (D)–(I) have been binned. Volume fractions ϕ are [(A), (D), and (G)] 0.575, [(B), (E), and (H)] 0.602, and [(C), (F), and (I)] 0.624.

2. *Recovery experiments*

Following the step-stress experiment, the rheometer imposed $\sigma = 0$ Pa. (For a quantitative characterization of the rheometer response, see the supplementary material [56].) While the stress was kept at $\sigma = 0$ Pa, the sample relaxed and the evolution of the recovered strain $\gamma_r(t)$ was measured [Figs. 4(D)–4(F)]. Again, a different behavior is observed depending on the initially applied stress.

For $\sigma > \sigma_{y,DSS}$, the recovered strain $\gamma_r(t)$ decays toward a plateau that indicates a magnitude of the total recovered strain $\gamma_{r,\infty}$ of about 10% with slightly more strain recovered for larger initially applied stresses. [For the largest initially applied stress and a volume fraction $\phi = 0.575$ and hence the sample with the lowest viscosity under shear, the measured recovered strain $\gamma_r(t)$ increases for long times, which we attribute to residual drift of the tool, which might also be responsible for the slight increase of $\gamma_r(t)$ at small times.] Although the application of a stress beyond the yield stress fluidizes the sample, the dynamics is still dominated by caging. The cages continuously break and reform but still suppress out-of-cage motions and hence at any instant restrict particle motions to about a tenth of the particle size. This constrains the extent to which structural deformations can be recovered and limits the magnitude of the maximally recoverable strain to about 10% [19]. This value is consistent with the observed $\gamma_{r,\infty} \approx 10\%$ and the absence of a strong dependence on the applied stress, as long as the stress is beyond the yield stress. The cage dynamics also limits the maximum sustainable deformation, i.e., the yield strain γ_y, which has a comparable value (Fig. 11 in Appendix A).

For $\sigma < \sigma_{y,DSS}$, the strain recovery, $\gamma_r(t)$, is much slower and smaller. Furthermore, it shows a more pronounced dependence on the initially applied stress. Since the sample did not yield, it behaves as a deformed solid with a mainly elastic response. It essentially recovers the imposed strain, which depends on the applied stress and the duration of the experiment.

The total recovered strain $\gamma_{r,\infty}$ can be compared to the maximum imposed strain $\gamma(t = 10^3\,s)$ (Fig. 5). If the applied stress is below the yield stress, $\sigma \lesssim \sigma_{y,DSS}$, the sample does not yield but remains solid-like and exhibits elastic behavior.

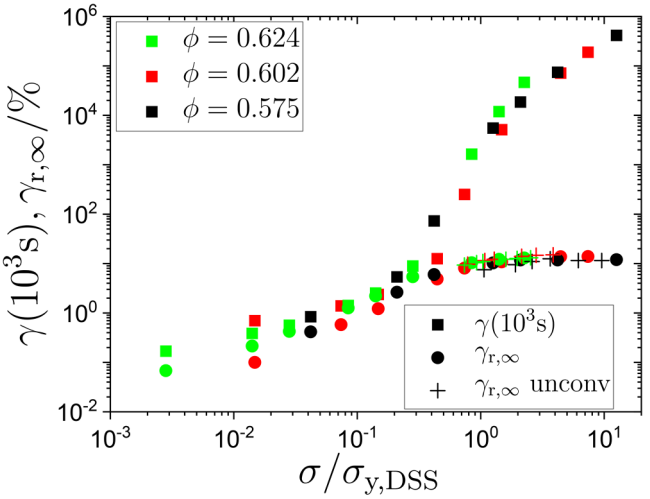

FIG. 5. Strain at the end of the creep measurement, i.e., maximum imposed strain $\gamma(t{=}10^3\,\mathrm{s})$ (squares) and magnitude of the total recovered strain after the cessation of stress, $\gamma_{r,\infty}$ (circles), as a function of applied stress σ normalized by the yield stress $\sigma_{y,DSS}$. Data were obtained in conventional experiments [Figs. 4(D)–4(F)], i.e., the application of a constant stress σ was followed by relaxation while $\sigma = 0\,\mathrm{Pa}$ (filled symbols), and unconventional experiments [Figs. 2(G)–2(I)], i.e., the application of a constant strain rate $\dot\gamma$ was followed by relaxation while $\sigma = 0\,\mathrm{Pa}$ (crosses). Volume fractions ϕ as indicated.

Accordingly, the strain is fully recovered, $\gamma_{r,\infty} \approx \gamma(10^3\,\mathrm{s})$. For stresses beyond the yield stress, $\sigma \gtrsim \sigma_{y,DSS}$, the sample is fluidized. The limited cage dynamics results in a saturation of the magnitude of the total recovered strain $\gamma_{r,\infty}$ to about 10%, as discussed above. In contrast, the maximum imposed strain $\gamma(10^3\,\mathrm{s})$ monotonically increases upon increasing the applied stress σ. For large applied stress, $\gamma(10^3\,\mathrm{s})$ increases linearly, i.e., $\gamma(t) = \dot\gamma t = (\sigma/\eta)t \sim \sigma$ due to the constant viscosity η of the fluidized sample [Figs. 4(A)–4(C)]. Thus, an increasingly small fraction of the imposed strain is recovered upon shear cessation. The transition between the two regimes is expected to occur at about the yield stress. It is indeed observed at about $0.5\sigma_{y,DSS} \approx \sigma_{y,fc}$ (Appendix A). We hence consider the conditions under which the yield stresses have been measured and compare them to the conditions under which the strain recovery is probed. To determine the recovered strain at about the transition, a constant stress of the order of the yield stress is applied until a steady state is reached and then the stress is released. The yield stress $\sigma_{y,fc}$ is determined based on the flow curve. The flow curve is obtained by applying a constant shear rate and measuring the stress once a steady state is reached (Sec. III C 1). For glasses, the flow curve exhibits a plateau at low strain rates, which is associated with the yield stress. Thus, $\sigma_{y,fc}$ is determined by applying a constant shear rate $\dot\gamma \to 0$. The yield stress $\sigma_{y,DSS}$ has been determined in dynamic strain sweeps (DSS) and hence under oscillatory deformation with an angular frequency $\omega = 1$ rad/s (Appendix A). This implies a higher shear rate than that relevant for the determination of $\sigma_{y,fc}$. Thus, $\sigma_{y,fc}$ has been determined under more similar conditions, constant application of shear and extrapolation to zero shear rate, and hence is more relevant here. This is consistent with the observation that the transition between the two regimes, $\gamma_{r,\infty} \approx \gamma(10^3\,\mathrm{s})$ and $\gamma_{r,\infty} \approx 10\%$, occurs at $\sigma_{y,fc}$ rather than at $\sigma_{y,DSS}$.

Oscillations are observed at $t \approx 0.1\,\mathrm{s}$ independent of the previously applied stress [Figs. 4(D)–4(F)]. The oscillations are analogous to those observed in the creep experiments [33,38,43,68]. They are also attributed to the interplay between instrument inertia and sample elasticity [74–76].

C. Strain vs stress-controlled experiments

1. Step-rate vs step-stress experiments

The step-rate and step-stress experiments (Secs. III A 1 and III B 1) both lead to a steady state if the sample yielded. The characteristics of these steady states can be compared to the flow curve. To determine the flow curve, decreasing shear rates were applied in the range $5 \times 10^{-4}\,\mathrm{s}^{-1} \lesssim \dot\gamma \lesssim 30\,\mathrm{s}^{-1}$, corresponding to $10^{-4} \lesssim \dot\gamma\tau_{B,0} \lesssim 7$ with the Brownian time $\tau_{B,0}$ (Sec. II A). At a given shear rate $\dot\gamma$, the stress σ was repeatedly measured for 30–60 s until the difference between three consecutive measurements was smaller than 5%, which is assumed to indicate that a steady state was reached. The resulting flow curves $\sigma(\dot\gamma)$ show the expected shape (Fig. 6, solid lines). For high shear rates, the stress increases with shear rate. The slope and hence the viscosity $\eta = \sigma/\dot\gamma$ decreases with shear rate indicating shear thinning [19,39,40,42,50,69,70]. Toward low shear rates, the stress tends to a plateau given by the yield stress $\sigma_{y,fc}$ for the samples with a volume fraction above the glass transition $\phi > \phi_g \approx 0.59$ (Table I in Appendix A). In contrast, the sample with $\phi < \phi_g$ exhibits a continuous decrease in the stress indicating flow at low shear rates.

The flow curve can be compared to the steady-state stress σ_{ss} measured in step-rate experiments with constant shear rate $\dot\gamma$ (Fig. 6, dotted lines and triangles). They show essentially the same dependence $\sigma_{ss}(\dot\gamma)$, although in a step-rate experiment a constant shear rate is imposed on an initially quiescent sample whereas the shear rate is successively changed to

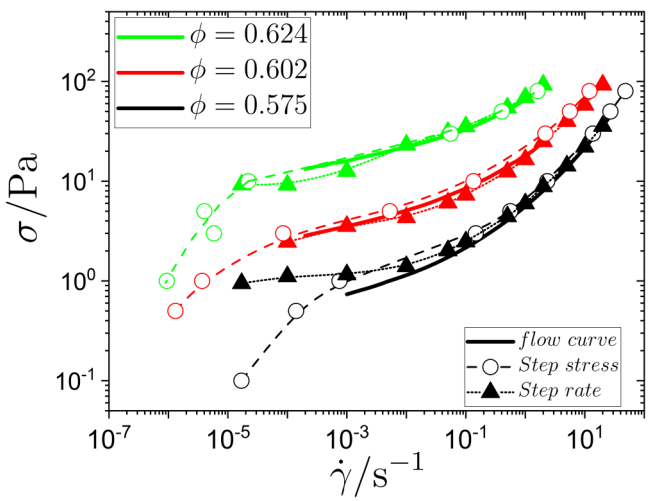

FIG. 6. Stress σ as a function of shear rate $\dot\gamma$ for different volume fractions ϕ as indicated. The data represent flow curve experiments (solid lines), the steady states of step-rate experiments [dotted lines, triangles, Figs. 2(A)–2(C)], and the final evolutions of step-stress experiments [dashed lines, open circles, Figs. 4(A)–4(C)].

determine the flow curve. For the lowest volume fraction sample, $\phi = 0.575$, the steady-state stress determined in step-rate experiments shows a plateau at low rates, in contrast to the steady-state stress in the flow curve. This indicates that a steady state might not have been reached during the determination of the flow curve or that the measurements were affected by slip. It has been reported [71–73] that near and above the glass transition, $\phi \gtrsim \phi_g$, slip can affect the measurements at small shear rates if smooth tools are used. In the present experiments, roughened tools are used to reduce slip but some slip cannot be excluded at low shear rates.

At the end of the step-stress (creep) experiments, the shear rate $\dot{\gamma}(10^3 s)$ was determined as a function of the applied stress σ. The observed $\sigma(\dot{\gamma})$ (Fig. 6, dashed lines and open circles) agrees with the flow curve for stresses beyond the yield stress, $\sigma > \sigma_{y,DSS}$, i.e., as long as the sample has been fluidized. This is despite the significant differences between the two experiments; a constant stress is imposed on an initially quiescent sample in a step-stress experiment whereas the shear rate was stepwise decreased to determine the flow curves. In contrast, if $\sigma < \sigma_{y,DSS}$, the applied stress is lower than observed in a flow curve or a step-rate experiment. This is necessarily the case for the samples with volume fractions $\phi > \phi_g$ since for small rates the flow curve tends to a minimum stress, the plateau at $\sigma_{y,fc} \approx \sigma_{y,DSS}$ (Appendix A). Although for $\sigma < \sigma_{y,DSS}$ the samples do not yield and flow, they deform and thus the strain and strain rate evolve with time [Figs. 4(A)–4(C)] meaning the value of the strain rate extracted depends on the time at which it was determined. Since the shear rate tends to decrease during the experiment, the drop of $\sigma(\dot{\gamma})$ toward small $\dot{\gamma}$ becomes less pronounced if the shear rate is extracted later.

As discussed above, the same dependence of the steady-state stress on the shear rate is observed regardless of whether initially a constant stress or constant rate was applied, if the sample yielded (Fig. 6). However, how the samples yield and reach a steady state follows different paths [38]. Therefore, we directly compare the transient behaviors during step-rate and step-stress experiments. In step-rate experiments, $\sigma(\gamma)$ is monitored for a fixed $\dot{\gamma}$ whereas in step-stress experiments, $\gamma(t)$ is followed for a given σ. To compare these two cases, $\sigma\dot{\gamma}(\gamma)$ is considered as a function of strain γ or, equivalently, time $t = \gamma/\dot{\gamma}$. The experimental parameters, a constant applied stress σ or shear rate $\dot{\gamma}$, are chosen to match according to the flow curve. In the steady state, i.e., at large strains or long times, hence the data from the step-rate and step-stress experiments coincide in the plateau (Fig. 7). However, the graphs $\sigma\dot{\gamma}(\gamma)$ evolve differently. The data from the step-stress experiments exhibit a slow increase whereas the data from the step-rate experiments increase faster and show a characteristic overshoot and an approach to the plateau from larger values. This means that in the step-rate experiments the plateau with the asymptotic value of $\sigma\dot{\gamma}(\gamma \to \infty)$ tends to be reached at smaller strains when compared with the step-stress cases. As indicated by the integral of $\sigma\dot{\gamma}(t)$, this involves a larger energy input, which is due to the faster increase and overshoot.

The step-stress data show a slight dip at $\gamma \approx 20\%$ [Fig. 7(A), arrow], which appears to correspond to the overshoot of the step-rate data. A series of increasing applied stresses σ reveals an overshoot followed by a dip for $\sigma \gtrsim \sigma_y$ [Fig. 7(A), inset]. As the applied stress increases, the overshoot and dip become less pronounced and shift to larger strains. This corresponds to the dependence of the magnitude and position of the overshoot in the measured stress $\sigma(t)$ in step-rate experiments [Fig. 2(A)]. In step-rate experiments, the decrease in the stress from the overshoot to the plateau reflects the release of stress initiated by yielding. Correspondingly, in the step-stress experiments, the overshoot and dip might also indicate yielding. They are attributed to the interplay between the instrument inertia and the elasticity of the yielded sample (Sec. III B 1) [74–76]. The (visco)elasticity of the yielded sample depends on the applied stress and hence the magnitude of the feature changes with the applied stress. For small stresses $\sigma \gtrsim \sigma_{y,DSS}$, the sample is just fluidized and oscillations are still visible whereas for larger stresses σ oscillations become less pronounced and eventually are no longer observed.

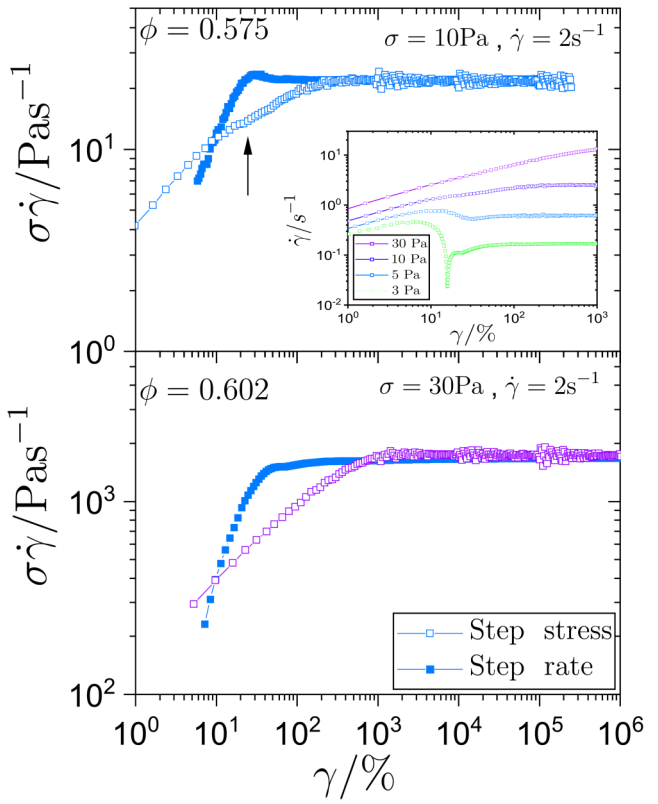

FIG. 7. Step-rate and step-stress data shown as stress times shear rate, $\sigma\dot{\gamma}$, as a function of strain γ for different applied shear rates $\dot{\gamma}$ and stresses σ, respectively, as well as for different volume fractions ϕ (as indicated). A slight dip in $\sigma\dot{\gamma}(\gamma)$ of the step-stress experiment is indicated by an arrow. In the inset, this feature is shown for more applied stresses σ (as indicated).

2. *Relaxation vs recovery*

After a step-rate experiment, usually the shear rate is fixed to $\dot{\gamma} = 0\,\text{s}^{-1}$ and the relaxation of the stress $\sigma(t)$ followed [Figs. 2(D)–2(F)]. Correspondingly, after a step-stress experiment, the stress is released and fixed to $\sigma = 0\,\text{Pa}$ and the

recovered strain $\gamma_r(t)$ measured [Figs. 4(D)–4(F)]. The observed relaxation might thus depend on the initial experiment, i.e., the application of a strain rate $\dot{\gamma}$ or a stress σ, or on the parameter kept fixed, i.e., $\dot{\gamma} = 0\,\mathrm{s}^{-1}$ or $\sigma = 0\,\mathrm{Pa}$, or on both. To disentangle the effect of the previous and concurrent treatment and to allow for a direct comparison, two additional types of experiments were performed (Fig. 1). First, a step-rate experiment was performed and then the stress fixed to $\sigma = 0\,\mathrm{Pa}$. To technically realize such a test, the constant shear rate was dropped to zero briefly (for 20 ms) and only then the stress was fixed to $\sigma = 0\,\mathrm{Pa}$ while the recovered strain $\gamma_r(t)$ was measured. Second, a step-stress experiment was performed and then the shear rate fixed to $\dot{\gamma} = 0\,\mathrm{s}^{-1}$. In detail, the constant stress was stopped by applying a stress in the opposite direction for a very short time (a few tens of ms) before the rheometer was commanded to fix the strain to $\gamma = 0$ (Appendix B and the supplementary material [56], especially Fig. S4). The stress relaxation data, $\sigma(t)$, are only considered once a negligible shear rate is reached. These procedures allow us to compare all combinations, i.e., shear is applied by strain rate or stress control and the relaxation observed under strain or stress control, the latter independent of whether a constant strain rate or constant stress was applied. Therefore, not only the effect of strain or stress control but also the effect of the previous treatment and hence sample history can be investigated.

The different recoveries of the strain $\gamma_r(t)$ have a common shape irrespective of whether initially a step-rate [Figs. 2(G)–2(I) and 8(A)–8(C), solid lines] or step-stress experiment [Figs. 4(D)–4(F) and 8(A)–8(C), dashed lines] was performed and even irrespective of yielding. This includes the oscillations at $t \approx 0.1$ s that are due to the interplay between instrument inertia, sample elasticity, and shear wave propagation [74–76]. The sequence of $\gamma_r(t)$ curves follows a consistent trend when taking into account the relation between the applied shear rate $\dot{\gamma}$ and the applied stress σ provided by the flow curve $\sigma(\dot{\gamma})$. This can be quantified by the total recovered strain $\gamma_{r,\infty}$. It agrees with the values observed in the conventional experiments, that is, the relaxation following a step-stress experiment (Fig. 5). Hence, strain recovery does not depend upon how the preceding steady state was reached. Even for samples that did not yield and did not reach a steady state, the recovered strain $\gamma_r(t)$ shows a similar shape. The strain recovery is, therefore, also independent of yielding. Nevertheless, the values of the magnitude of the total recovered strain $\gamma_{r,\infty}$ after step-stress tests with $\sigma < \sigma_y$ cannot be quantitatively compared to the values determined after step-rate tests because the flow curve does

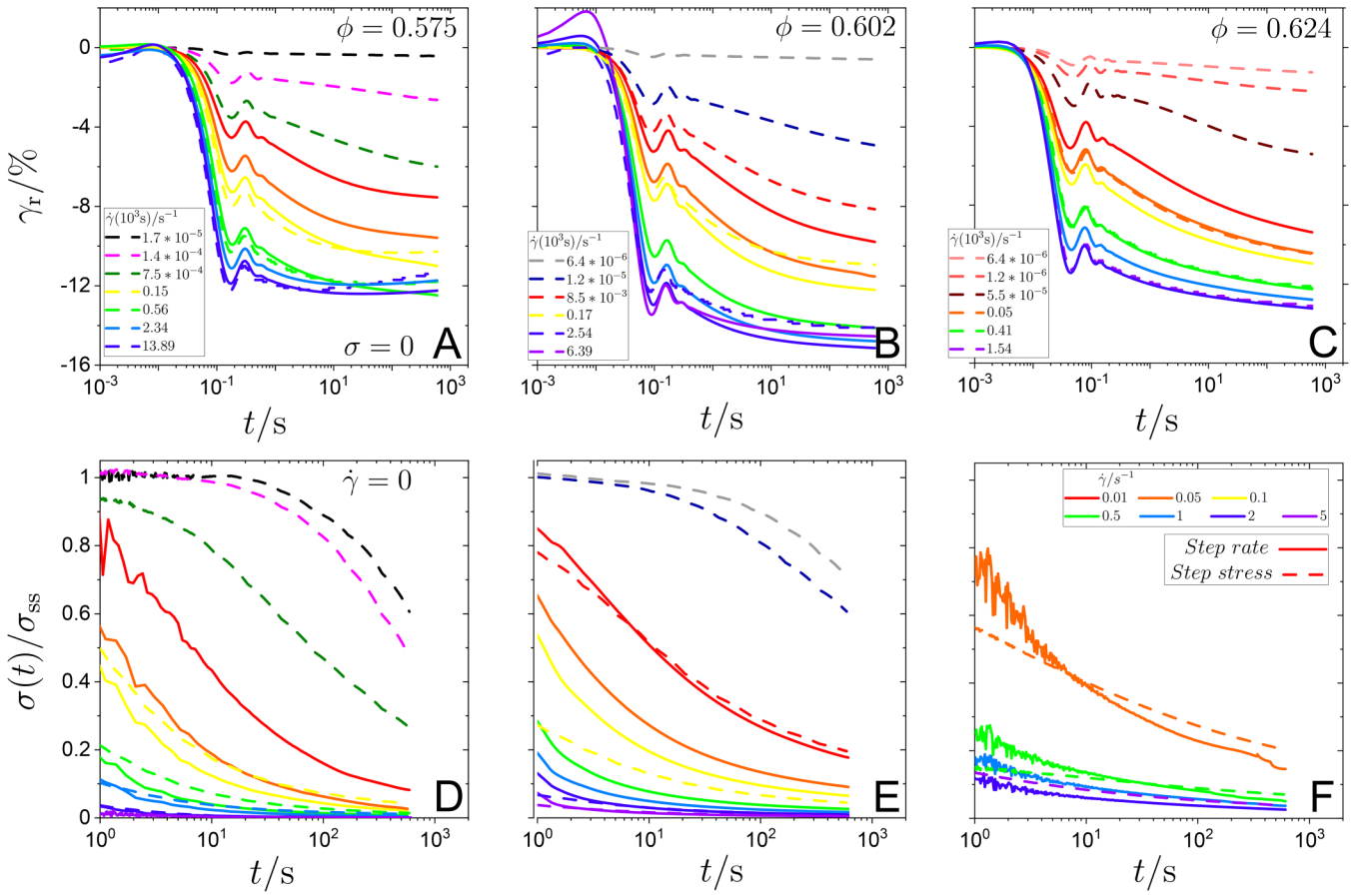

FIG. 8. (A)–(C) Recovered strain $\gamma_r(t)$ while the stress is set to zero, $\sigma = 0\,\mathrm{Pa}$ [Figs. 2(G)–2(I) and 4(D)–4(F)] and (D)–(F) relaxed stress $\sigma(t)$ normalized by the steady-state stress σ_{ss} while the shear rate is set to zero, $\dot{\gamma} = 0\,\mathrm{s}^{-1}$ [Figs. 2(D)–2(F) and 4(G)–4(I)], as a function of time t after a constant shear rate $\dot{\gamma}$ (solid lines) or a constant stress σ (dashed lines) has been applied and released. The shear rates applied in the step-rate experiments, $\dot{\gamma}$, and the shear rates at the end of the step-stress experiment, $\dot{\gamma}(t{=}10^3\mathrm{s})$, are indicated. Volume fractions ϕ are [(A) and (D)] 0.575, [(B) and (E)] 0.602, and [(C) and (F)] 0.624.

not allow applied stresses below the yield stress to be related to a shear rate $\dot{\gamma}$.

In contrast to strain recovery, the relaxation of the stress $\sigma(t)$ shows two distinct shapes [Figs. 8(D)–8(F)]. If the sample did not yield, the shape is concave in the observed time window while, if the sample yielded and was flowing, the shape is convex. In the latter case, it appears irrelevant whether a steady state was reached by applying a constant shear rate [Figs. 2(D)–2(F) and 8(D)–8(F), solid lines] or a constant stress [Figs. 4(G)–4(I) and 8(D)–8(F), dashed lines]. The time dependence of the relaxed stress $\sigma(t)$ is identical and the extent of the stress relaxation follows a common trend taking into account the flow curve $\sigma(\dot{\gamma})$. The data also allow for the calculation of the components of the stress relaxation, the hydrodynamic, σ_h, Brownian, σ_B, and residual, σ_r, stress as a function of the applied stress σ, which can again be associated with a shear rate $\dot{\gamma}$ using the flow curve $\sigma(\dot{\gamma})$. Their values quantitatively agree with the values determined during the relaxation following a step-rate experiment (Fig. 3), except the Brownian and residual stresses of the sample with the lowest volume fraction $\phi = 0.575$. In this case, the deviations are larger than the experimental uncertainties and might be due to the experimental procedure and hence a technical reason. In addition, the sample below and the samples above the glass transition might respond differently to the application of a constant shear rate and a constant stress which only becomes apparent during stress relaxation. Nevertheless, apart from these differences, the stress relaxation $\sigma(t)$ appears to a large extent independent of how the steady state has been reached, but a steady state needs to be reached.

The yielded samples appear to relax in a similar, although not identical way, independent of whether the stress [Figs. 8(A)–8(C)] or the shear rate [Figs. 8(D)–8(F)] is set to zero, except for the different response times of the rheometers and the oscillations at early times in the strain recovery data. To allow for a direct comparison, we focus on the relaxation for times $t \geq 1$ s and consider step-rate experiments. Moreover, dimensionless quantities are considered. For $\dot{\gamma} = 0\,\mathrm{s}^{-1}$, the stress decays from the steady-state stress σ_{ss} to the residual stress σ_r. We consider part of this decay, from $\sigma(1\mathrm{s})$ to σ_r, and hence the fraction $\hat{\sigma}(1\mathrm{s}) = (\sigma(1\mathrm{s}) - \sigma_r)/(\sigma_{ss} - \sigma_r)$. Since the residual stress σ_r is very small compared to the steady-state stress, $10^{-5} < \sigma_r/\sigma_{ss} < 10^{-1}$ [Fig. 3(C)], $\hat{\sigma}(1\mathrm{s}) \approx \sigma(1\mathrm{s})/\sigma_{ss}$. This is approximately the scaled Brownian stress [Fig. 3(C)]. Accordingly, the fraction $\hat{\sigma}(1\mathrm{s})$ is found to decrease with shear rate $\dot{\gamma}$ (Fig. 9). For $\sigma = 0$ Pa, the sample relaxes the total recovered strain $\gamma_{r,\infty}$ and hence we consider the fraction of the decay, $\hat{\gamma}_r(1\mathrm{s}) = (\gamma_{r,\infty} - |\gamma_r(1\mathrm{s})|)/\gamma_{r,\infty}$. The fraction $\hat{\gamma}_r(1\mathrm{s})$ decreases with shear rate $\dot{\gamma}$ (Fig. 9). This reflects the increasing initial decay caused by instrument inertia effects that result in oscillations and become more pronounced mainly due to technical reasons [74–76]. Similar fractions of the strain, $\hat{\gamma}_r(1\mathrm{s})$, and of the stress, $\hat{\sigma}(1\mathrm{s})$, are relaxed at long times beyond $\dot{\gamma}\tau_{B,\phi} \approx 1$ and 10 for the less ($\phi < \phi_g$) and more ($\phi > \phi_g$) concentrated samples, respectively. While this seems an interesting experimental observation, the reason and the implications are not clear.

The long-time decays ($t \geq 1$ s) are compared based on the reduced relaxed stress $\hat{\sigma}(t) = (\sigma(t) - \sigma_r)/(\sigma_{ss} - \sigma_r) \approx \sigma(t)/\sigma_{ss}$ and the reduced recovered strain $\hat{\gamma}_r(t)[\hat{\sigma}(1\mathrm{s})/\hat{\gamma}_r(1\mathrm{s})]$ for the sample with $\phi = 0.575$ (Fig. 10). As expected, the magnitude of the decays depends on the initially applied shear rate $\dot{\gamma}$. However, the relaxations occur on a similar time scale. Hence, it seems less important whether the relaxation occurs while $\sigma = 0$ Pa or $\dot{\gamma} = 0\,\mathrm{s}^{-1}$. In both cases, no time scale is imposed and hence the particle relaxation provides the only relevant time scale. The considered slow decay is due to the relaxation of the shear-induced

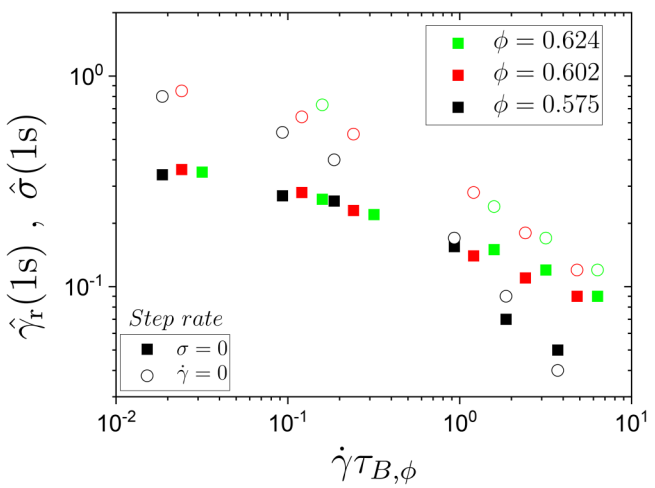

FIG. 9. Fractions of the long-time relaxation, namely, long-time strain recovery, $\hat{\gamma}_r(1\mathrm{s}) = (\gamma_{r,\infty} - |\gamma_r(1\mathrm{s})|)/\gamma_{r,\infty}$ (filled squares), where $\gamma_r(1\mathrm{s})$ is the strain recovered after 1 s and $\gamma_{r,\infty}$ the magnitude of the total recovered strain and fraction of the long-time stress relaxation, $\hat{\sigma}(1\mathrm{s}) = (\sigma(1\mathrm{s}) - \sigma_r)/(\sigma_{ss} - \sigma_r)$ (open circles), where $\sigma(1\mathrm{s})$ is the stress relaxed after 1 s, σ_r is the residual stress, and σ_{ss} is the steady-state stress. Both are shown as functions of the shear rate $\dot{\gamma}$ normalized by the Brownian time $\tau_{B,\phi}$. The sample was fluidized by applying a constant shear rate and the relaxation was followed while the shear rate (open circles) or stress (filled squares) was set to zero. Volume fractions ϕ as indicated.

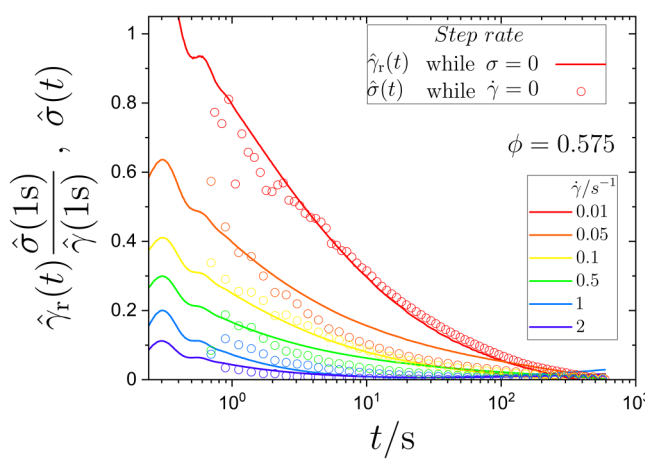

FIG. 10. Reduced relaxed stress $\hat{\sigma}(t) \approx \sigma(t)/\sigma_{ss}$ (open circles) and reduced recovered strain $\hat{\gamma}_r(t)[\hat{\sigma}(1\mathrm{s})/\hat{\gamma}_r(1\mathrm{s})]$ (solid lines) as a function of time t while the shear rate (open circles) or the stress (solid lines) has been set to zero after a constant shear rate $\dot{\gamma}$ (as indicated) has been applied and released. The same data as in Figs. 2(D) and 2(G) but represented differently. Volume fraction $\phi = 0.575$.

anisotropic particle arrangement and related to the Brownian stress. For the sample with volume fraction $\phi = 0.575$, the Brownian time $\tau_{B,\phi} = 1.86\,\mathrm{s}$ (Sec. II A), which is close to the time scale of the decay, a few seconds (Fig. 10). Nevertheless, also noticeable differences exist between the relaxations while σ or $\dot{\gamma}$ was set to zero. They are attributed to the different treatments of the sample. Under strain control, the sample is restrained to its macroscopic shape and the particles can only microscopically rearrange to relax stress whereas under stress control the sample can change its overall shape allowing deformations to relax through an overall macroscopic motion in addition to internal microscopic particle motions.

IV. CONCLUSIONS

The rheological response of hard sphere suspensions with concentrations around the glass transition was investigated during start-up and relaxation tests. Of particular interest was the comparison of strain and stress controlled experiments as well as the consequences of a previous application of strain or stress on the rheological properties in the steady state and the subsequent relaxation and hence of the sample history. An obvious difference between the two tests is the possibility of yielding. While in step-rate experiments yielding can always be achieved, in step-stress experiments yielding and flow only occur if the applied stress σ is beyond the yield stress σ_y.

Independent of the application of a strain rate or a stress beyond the yield stress, steady states are reached, in which the rheological properties are identical and agree with the flow curve obtained by a stepwise change of the strain rate. In contrast, for $\sigma < \sigma_y$, no steady state is reached and the strain keeps evolving. Thus, the data do not resemble the flow curve and, in particular, no plateau is observed at small shear rates.

Different paths toward the steady state were observed which are compared considering $\sigma\dot{\gamma}(t)$. The approach is faster and contains a characteristic overshoot in step-rate experiments. In step-stress experiments, the approach is slower and can be achieved with a smaller energy input. A detailed comparison reveals an overshoot followed by a dip of $\sigma\dot{\gamma}(t)$ in the step-stress experiments. This feature is most pronounced for stresses $\sigma \gtrsim \sigma_y$ and becomes less pronounced and moves to larger strains as σ is increased. It corresponds to the overshoot in $\sigma\dot{\gamma}(t)$ observed in step-rate experiments and thus indicates yielding. Its position can hence provide a measure of the yield strain.

To study the relaxation after shear cessation, a step-rate test is usually followed by setting the shear rate to zero and, correspondingly, after a step-stress test the stress is set to zero. To explore all possible combinations, we also set the stress to zero after a step-rate test and set the shear rate to zero after a step-stress test. Independent of the previous treatment, in all cases, the recovered strain $\gamma_r(t)$ follows a similar trend, even if no steady state was reached and no yielding occurred and hence the sample behaved solid-like. The magnitude of the total recovered strain $\gamma_{r,\infty}$ increases with the applied stress or strain rate but saturates at about 10%, which coincides with the extent of in-cage motions. This trend is also independent of the previous treatment. In contrast, the relaxed stress $\sigma(t)$ shows qualitatively different shapes depending on whether a steady state was reached or not. If a steady state was reached, the contributions to the relaxed stress $\sigma(t)$, namely, the hydrodynamic σ_h, Brownian σ_B, and residual σ_r stresses are independent of the previous treatment. The hydrodynamic stress increases approximately linearly with shear rate and approaches the steady-state stress. At large shear rates, $\dot{\gamma}\tau_{B,\phi} \gtrsim 1$, it dominates the Brownian stress, which moderately decreases with shear rate. The relatively small contribution of the residual stress decreases with increasing shear rate. If normalized by the steady-state stress σ_{ss}, the hydrodynamic and Brownian stresses are independent of the volume fraction, whereas the normalized residual stress is not.

The reduced relaxed stress $\hat{\sigma}(t)$ and the reduced recovered strain $\hat{\gamma}_r(t)$ allow for a direct comparison of the relaxation while either the strain or the stress is set to zero. Despite the different conditions, the long-time decay occurs on a similar time scale and with a common time dependence. Nevertheless, there are also small but noticeable deviations.

These observations confirm the importance of yielding to reach a steady state. The unambiguous identification of a steady state requires not only macroscopic rheological data but also mesoscopic and microscopic information on, e.g., the particle arrangement and dynamics as well as the flow profile. Here, however, we only characterized the steady states rheologically. This seems to be sufficient to define the steady state with respect to the rheological response upon shear cessation, which was found to be independent of the shear history. Nevertheless, a microscopic study would be valuable to directly provide the information required to identify the steady state unambiguously.

ACKNOWLEDGMENTS

We thank the Center for Advanced Imaging (University Düsseldorf) for help with the SEM experiments. Support from the Deutsche Forschungsgemeinschaft (DFG) and the Alexander von Humboldt Foundation is acknowledged.

APPENDIX A: DETERMINATION OF THE YIELD STRESS

The yield stress σ_y was determined in oscillatory experiments and based on flow curves.

In the DFS, an oscillatory deformation was applied with the strain amplitude in the linear regime, $\gamma = 0.3\%$, and a

TABLE I. Yield stress for different volume fractions ϕ as determined by DSS, $\sigma_{y,DSS}$, and flow curve measurements, $\sigma_{y,fc}$.

ϕ	$\sigma_{y,DSS}$ (Pa)	$\sigma_{y,fc}$ (Pa)
0.575	2.38	—
0.602	6.76	3.6
0.624	35.52	16.7

varying angular frequency $0.02\,\mathrm{rad/s} \leq \omega \leq 50\,\mathrm{rad/s}$ corresponding to $0.004 \lesssim \omega\tau_{B,0} \lesssim 11$, where $\tau_{B,0}$ is the Brownian time (Sec. II A). This frequency range is not expected to be affected by instrument or sample inertia nor by shear wave propagation effects, which are only predicted to be noticeable for frequencies $\omega > 100\,\mathrm{rad/s}$ [74–77]. Within the explored range of angular frequencies ω, the value of the elastic modulus G' is almost constant with only a weak increase toward large ω, whereas the increase in the viscous modulus G'' starts at smaller values of ω and is more pronounced [Fig. 11(A)]. The elastic response dominates the viscous response, $G' > G''$, at all frequencies ω. These dependencies are characteristic for concentrated colloidal suspensions, including colloidal glasses [26,51,78,79]. The qualitative behavior is independent of ϕ. However, the magnitude of the moduli shows a strong increase with ϕ, which is indicative of particle–particle interactions that resemble hard sphere interactions [36,51,80,81]. Moreover, the absolute values of the normalized modulus $G'/(k_BT/R^3)$ quantitatively agree with previous data [36].

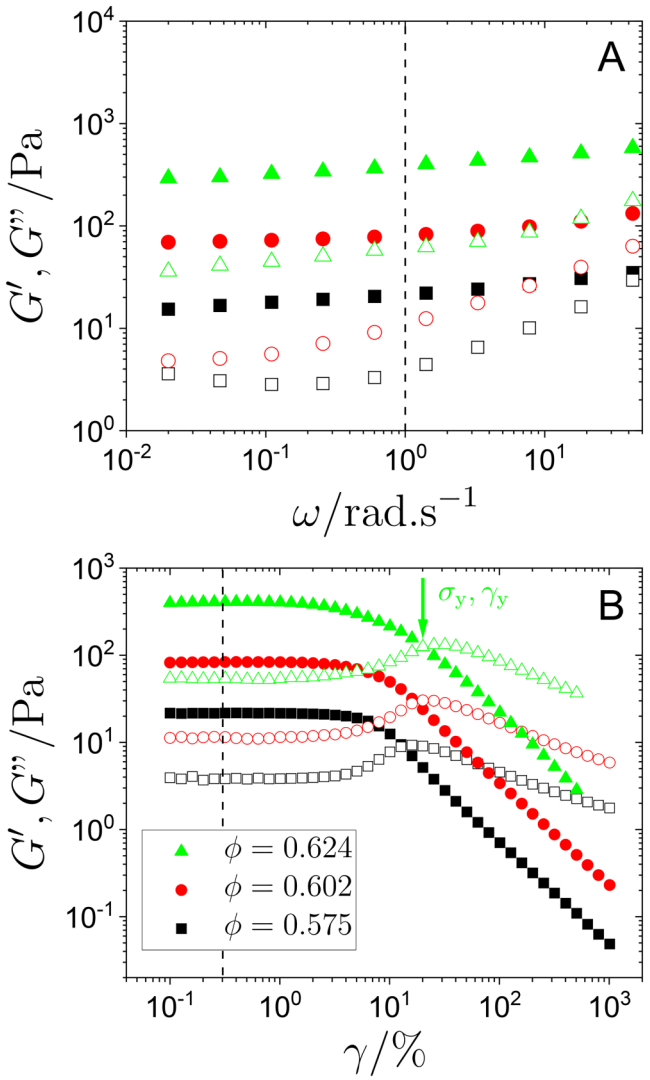

FIG. 11. (A) DFS with strain amplitude $\gamma = 0.3\%$ and (B) DSS with angular frequency $\omega = 1.0\,\mathrm{rad/s}$. Elastic G' (solid symbols) and viscous G'' (open symbols) moduli as a function of angular frequency ω and strain amplitude γ, respectively. The arrow marks the yield point ($\gamma_{y,DSS}$, $\sigma_{y,DSS}$), defined by $G' = G''$, of the sample with $\phi = 0.624$. The vertical dashed lines indicate the angular frequency and strain amplitude applied in the DFS and DSS, respectively. Volume fractions ϕ as indicated.

The DFS were complemented by DSS with an angular frequency in the linear regime, $\omega = 1.0\,\mathrm{rad/s}$ [Fig. 11(A), dashed line]. The DSS experiments covered strain amplitudes $0.1\% \leq \gamma \leq 1000\%$. The same qualitative behavior is observed but with increasing ϕ the magnitudes of G' and G'' increase and the features shift to slightly larger strain amplitudes γ [Fig. 11(B)]. At small strain amplitudes $\gamma \lesssim 2\%$, G' and G'' are approximately constant indicating the linear regime. At large γ, nonlinear shear-thinning and viscoelastic fluid-like behavior is observed. This agrees with the prediction of the Maxwell model for hard spheres in the flow regime modified to include the yield stress [82–84]. The crossover between these two regimes is considered to occur when $G' = G''$ [Fig. 11(B), arrow] [22,23]. The corresponding strain amplitude $\gamma_{y,DSS} \approx 10\%$–$20\%$ can be taken as a measure of the yield strain and the stress $\sigma_{y,DSS}$ as a measure of the yield stress (Table I). The yield stress $\sigma_{y,DSS}$ increases with volume fraction ϕ.

The flow curves $\sigma(\dot{\gamma})$ have been determined for all volume fractions ϕ (Sec. III C 1, Fig. 6). For samples with $\phi > \phi_g$, the yield stress $\sigma_{y,fc}$ has been extracted as the plateau value at low shear rates following the Herschel–Bulkley model [22,23] (Table I).

The values of the yield stress obtained by DSS, $\sigma_{y,DSS}$, are about twice the values determined based on the flow curves, $\sigma_{y,fc}$ (Table I). This difference is attributed to the different definitions and hence conditions under which the yield stresses were determined. To determine the flow curve, a constant shear rate was applied and the stress measured in the steady state. The yield stress was then associated with the plateau value at small shear rates, which develops in the case of glasses. In the DSS experiments, however, oscillatory shear was applied and hence the shear rate changed periodically. The yield stress is defined by the transition from solid-like behavior ($G' < G''$) at small strain amplitudes ($\gamma \lesssim 10\%$) to fluid-like behavior ($G' > G''$) at large strain amplitudes. Thus, the yield stress was determined at finite frequencies and thus finite average shear rates whereas the determination through the flow curve was based on an extrapolation to zero shear rate. At larger shear rates, the flow curve indicates a larger stress, $\sigma > \sigma_{y,fc}$, consistent with the observation that $\sigma_{y,DSS} > \sigma_{y,fc}$. Therefore, $\sigma_{y,fc}$ is more relevant to the present start-up and relaxation experiments. Nevertheless, for consistency, we use $\sigma_{y,DSS}$ to normalize the data because its determination can be extended to concentrated fluids with volume fractions $\phi < \phi_g$. In this case, the condition $G' = G''$ indicates the stress required to fluidize temporary cages, i.e., to eliminate the transient solid-like response at intermediate frequencies of a sample that already exhibits a fluid-like response at low frequencies.

APPENDIX B: RESPONSE OF RHEOMETERS

Both, the start-up and cessation of shear, ideally involve sudden changes of the applied stress or shear rate. It is hence crucial to take into account the response time of the

rheometers. In particular, the shear rate cannot be changed abruptly. The actually applied shear rate was followed upon commanding the rheometer to apply a constant shear rate and, for the cessation experiments, to set the shear rate to zero. Only data recorded after the desired shear was approximately reached were considered and are shown in the corresponding figures. In the supplementary material [56], the measured responses of the used rheometers and geometries are presented, analyzed, and discussed for representative examples.

REFERENCES

[1] Hunter, G. L., and E. R. Weeks, "The physics of the colloidal glass transition," Rep. Prog. Phys. **75**, 066501 (2012).

[2] Pusey, P. N., "Colloidal glasses," J. Phys.: Condens. Matter **20**, 494202 (2008).

[3] Pusey, P. N., Colloidal suspensions, in *Liquids, Freezing and the Glass Transition*, Nato Advanced Study Institute at Les Houches, Session LI, edited by J. P. Hansen, D. Levesque, and J. Zinn-Justin (North-Holland, Amsterdam, 1991), pp. 763–942.

[4] Pusey, P. N., and W. van Megen, "Observation of a glass transition in suspensions of spherical colloidal particles," Phys. Rev. Lett. **59**, 2083–2086 (1987).

[5] van Megen, W., T. C. Mortensen, S. R. Williams, and J. Müller, "Measurement of the self-intermediate scattering function of suspensions of hard spherical particles near the glass transition," Phys. Rev. E **58**, 6073–6085 (1998).

[6] Crassous, J. J., M. Siebenbürger, M. Ballauff, M. Drechsler, D. Hajnal, O. Henrich, and M. Fuchs, "Shear stresses of colloidal dispersions at the glass transition in equilibrium and in flow," J. Chem. Phys. **128**, 204902 (2008).

[7] Siebenbürger, M., M. Fuchs, H. H. Winter, and M. Ballauff, "Viscoelasticity and shear flow of concentrated, noncrystallizing colloidal suspensions: Comparison with mode-coupling theory," J. Rheol. **53**, 707–726 (2009).

[8] Joshi, Y. M., and G. Petekidis, "Yield stress fluids and aging," Rheol. Acta **57**, 521–549 (2018).

[9] Bandyopadhyay, R., P. H. Mohan, and Y. M. Joshi, "Stress relaxation in aging soft colloidal glasses," Soft Matter **6**, 1462–1466 (2010).

[10] Joshi, Y. M., "A model for aging under deformation field, residual stresses and strains in soft glassy materials," Soft Matter **11**, 3198–3214 (2015).

[11] Voigtmann, T., M. Siebenbürger, C. P. Amann, S. U. Egelhaaf, S. Fritschi, M. Krüger, M. Laurati, K. J. Mutch, and K. H. Samwer, "Rheology of colloidal and metallic glass formers," Colloid Polym. Sci. **298**, 681–696 (2020).

[12] Oswald, P., *Rheophysics: The Deformation and Flow of Matter* (Cambridge University, Cambridge, 2009).

[13] Fuchs, M., Nonlinear rheological properties of dense colloidal dispersions close to a glass transition under steady shear, in *Advances in Polymer Science* (Springer, New York, 2010), Vol. 236, pp. 55–115.

[14] Voigtmann, T., "Nonlinear glassy rheology," Curr. Opin. Colloid Interface Sci. **19**, 549–560 (2014).

[15] Kobelev, V., and K. S. Schweizer, "Strain softening, yielding and shear thinning in glassy colloidal suspensions," Phys. Rev. E **71**, 021401 (2005).

[16] Brady, J. F., "The rheological behavior of concentrated colloidal dispersions," J. Chem. Phys. **99**, 567–581 (1993).

[17] Sentjabrskaja, T., M. Hermes, W. C. K. Poon, C. D. Estrada, R. Castaneda-Priego, S. U. Egelhaaf, and M. Laurati, "Transient dynamics during stress overshoots in binary colloidal glasses," Soft Matter **10**, 6546–6555 (2014).

[18] Ballauff, M., J. M. Brader, S. U. Egelhaaf, M. Fuchs, J. Horbach, N. Koumakis, M. Krüger, M. Laurati, K. J. Mutch, G. Petekidis, M. Siebenbürger, T. Voigtmann, and J. Zausch, "Residual stresses in glasses," Phys. Rev. Lett. **110**, 215701 (2013).

[19] Petekidis, G., D. Vlassopoulos, and P. N. Pusey, "Yielding and flow of sheared colloidal glasses," J. Phys.: Condens. Matter **16**, S3955–S3963 (2004).

[20] Pham, K. N., G. Petekidis, D. Vlassopoulos, S. U. Egelhaaf, P. N. Pusey, and W. C. K. Poon, "Yielding of colloidal glasses," Europhys. Lett. **75**, 624–630 (2006).

[21] Pham, K. N., G. Petekidis, D. Vlassopoulos, S. U. Egelhaaf, W. C. K. Poon, and P. N. Pusey, "Yielding behavior of repulsion- and attraction-dominated colloidal glasses," J. Rheol. **52**, 649–676 (2008).

[22] Mewis, J., and N. J. Wagner, *Colloidal Suspension Rheology* (Cambridge University, New York, 2012).

[23] Larson, R. G., *The Structure and Rheology of Complex Fluids* (Oxford University, New York, 1999).

[24] Dullaert, K., and J. Mewis, "Stress jumps on weakly flocculated dispersions: Steady state and transient results," J. Colloid Interface Sci. **287**, 542–551 (2005).

[25] Sentjabrskaja, T., A. R. Jacob, S. U. Egelhaaf, G. Petekidis, T. Voigtmann, and M. Laurati, "Binary colloidal glasses: Linear viscoelasticity and its link to the microscopic structure and dynamics," Soft Matter **15**, 2232–2244 (2019).

[26] Mason, T. G., and D. A. Weitz, "Linear viscoelasticity of colloidal hard sphere suspensions near the glass transition," Phys. Rev. Lett. **75**, 2770–2773 (1995).

[27] Eisenmann, C., C. Kim, J. Mattsson, and D. A. Weitz, "Shear melting of a colloidal glass," Phys. Rev. Lett. **104**, 035502 (2010).

[28] Christopoulou, C., G. Petekidis, B. Erwin, M. Cloitre, and D. Vlassopoulos, "Ageing and yield behaviour in model soft colloidal glasses," Philos. Trans. R. Soc. A **367**, 5051–5071 (2009).

[29] Sentjabrskaja, T., R. Babaliari, J. Hendricks, M. Laurati, G. Petekidis, and S. U. Egelhaaf, "Yielding of binary colloidal glasses," Soft Matter **9**, 4524–4533 (2013).

[30] Petekidis, G., A. Moussaïd, and P. N. Pusey, "Rearrangements in hard-sphere glasses under oscillatory shear strain," Phys. Rev. E **66**, 051402 (2002).

[31] Petekidis, G., P. N. Pusey, A. Moussaïd, S. Egelhaaf, and W. C. K. Poon, "Shear-induced yielding and ordering in concentrated particle suspensions," Physica A **306**, 334–342 (2002).

[32] Sentjabrskaja, T., D. Guu, M. P. Lettinga, S. U. Egelhaaf, and M. Laurati, AIP Conf. Proc. **1518**, 206–213 (2013).

[33] Ballesta, P., and G. Petekidis, "Creep and aging of hard-sphere glasses under constant stress," Phys. Rev. E **93**, 042613 (2016).

[34] Siebenbürger, M., M. Ballauff, and T. Voigtmann, "Creep in colloidal glasses," Phys. Rev. Lett. **108**, 255701 (2012).

[35] Mutch, K. J., M. Laurati, C. P. Amann, M. Fuchs, and S. U. Egelhaaf, "Time-dependent flow in arrested states—Transient behaviour," Eur. Phys. J. Spec. Top. **222**, 2803–2817 (2013).

[36] Koumakis, N., A. Pamvouxoglou, A. S. Poulos, and G. Petekidis, "Direct comparison of the rheology of model hard and soft particle glasses," Soft Matter **8**, 4271–4284 (2012).

[37] Koumakis, N., M. Laurati, A. R. Jacob, K. Mutch, A. Abdellali, A. B. Schofield, S. U. Egelhaaf, J. F. Brady, and G. Petekidis, "Start-up shear of concentrated colloidal hard spheres: Stresses, dynamics and structure," J. Rheol. **60**, 603–623 (2016).

[38] Sentjabrskaja, T., J. Hendricks, A. R. Jacob, G. Petekidis, S. U. Egelhaaf, and M. Laurati, "Binary colloidal glasses under

transient stress- and strain-controlled shear," J. Rheol. **62**, 149–159 (2018).

[39] Zausch, J., J. Horbach, M. Laurati, S. U. Egelhaaf, J. M. Brader, T. Voigtmann, and M. Fuchs, "From equilibrium to steady state: The transient dynamics of colloidal liquids under shear," J. Phys.: Condens. Matter **20**, 404210 (2008).

[40] Laurati, M., K. J. Mutch, N. Koumakis, J. Zausch, C. P. Amann, A. B. Schofield, G. Petekidis, J. F. Brady, J. Horbach, M. Fuchs, and S. U. Egelhaaf, "Transient dynamics in dense colloidal suspensions under shear: Shear rate dependence," J. Phys.: Condens. Matter **24**, 464104 (2012).

[41] Jacob, A. R., A. S. Poulos, S. Kim, J. Vermant, and G. Petekidis, "Convective cage release in model colloidal glasses," Phys. Rev. Lett. **115**, 218301 (2015).

[42] Koumakis, N., M. Laurati, S. U. Egelhaaf, J. F. Brady, and G. Petekidis, "Yielding of hard-sphere glasses during start-up shear," Phys. Rev. Lett. **108**, 098303 (2012).

[43] Sentjabrskaja, T., P. Chaudhuri, M. Hermes, W. C. K. Poon, J. Horbach, S. U. Egelhaaf, and M. Laurati, "Creep and flow of glasses: Strain response linked to the spatial distribution of dynamical heterogeneities," Sci. Rep. **5**, 011884 (2015).

[44] Divoux, T., C. Barentin, and S. Manneville, "Stress overshoot in a simple yield stress fluid: An extensive study combining rheology and velocimetry," Soft Matter **7**, 9335–9349 (2011).

[45] Chaudhuri, P., and J. Horbach, "Onset of flow in a confined colloidal glass under an imposed shear stress," Phys. Rev. E **88**, 040301 (2013).

[46] Rosti, J., J. Koivisto, L. Laurson, and M. J. Alava, "Fluctuations and scaling in creep deformation," Phys. Rev. Lett. **105**, 100601 (2010).

[47] Andrade, E. N. D. C., "On the viscous flow in metals, and allied phenomena," Proc. R. Soc. A: Math. Phys. Eng. Sci. **84**, 1–12 (1910).

[48] Koumakis, N., E. Moghimi, R. Besseling, W. C. K. Poon, J. F. Brady, and G. Petekidis, "Tuning colloidal gels by shear," Soft Matter **11**, 4640–4648 (2015).

[49] Royall, C. P., W. C. K. Poon, and E. R. Weeks, "In search of colloidal hard spheres," Soft Matter **9**, 17–27 (2013).

[50] Koumakis, N., J. F. Brady, and G. Petekidis, "Complex oscillatory yielding of model hard-sphere glasses," Phys. Rev. Lett. **110**, 178301 (2013).

[51] Koumakis, N., A. B. Schofield, and G. Petekidis, "Effects of shear induced crystallization on the rheology and ageing of hard sphere glasses," Soft Matter **4**, 2008–2018 (2008).

[52] Schaertl, W., and H. Sillescu, "Brownian dynamics of polydisperse colloidal hard spheres: Equilibrium structures and random close packings," J. Stat. Phys. **77**, 1007–1025 (1994).

[53] Farr, R. S., and R. D. Groot, "Close packing density of polydisperse hard spheres," J. Chem. Phys. **131**, 244104 (2009).

[54] Desmond, K. W., and E. R. Weeks, "Influence of particle size distribution on random close packing of spheres," Phys. Rev. E **90**, 022204 (2014).

[55] Poon, W. C. K., E. R. Weeks, and C. P. Royall, "On measuring colloidal volume fractions," Soft Matter **8**, 21–30 (2012).

[56] See the supplementary material at https://www.scitation.org/doi/suppl/10.1122/8.0000212 for a determination, analysis, and discussion of the response of the rheometers.

[57] Marenne, S., J. F. Morris, D. R. Foss, and J. F. Brady, "Unsteady shear flows of colloidal hard-sphere suspensions by dynamic simulation," J. Rheol. **61**, 477–501 (2017).

[58] Ong, E. Y. X., M. Ramaswamy, R. Niu, N. Y. C. Lin, A. Shetty, R. N. Zia, G. H. McKinley, and I. Cohen, "Stress decomposition in LAOS of dense colloidal suspensions," J. Rheol. **64**, 343–351 (2020).

[59] Foss, D. R., and J. F. Brady, "Structure, diffusion and rheology of Brownian suspensions by Stokesian dynamics simulations," J. Fluid Mech. **407**, 167–200 (2000).

[60] Lin, N. Y. C., B. M. Guy, M. Hermes, C. Ness, J. Sun, W. C. K. Poon, and I. Cohen, "Hydrodynamic and contact contributions to continuous shear thickening in colloidal suspensions," Phys. Rev. Lett. **115**, 228304 (2015).

[61] O'Brien, V. T., and M. E. Mackay, "Stress components and shear thickening of concentrated hard sphere suspensions," Langmuir **16**, 7931–7938 (2000).

[62] Jacob, A. R., E. Moghimi, and G. Petekidis, "Rheological signatures of aging in hard sphere colloidal glasses," Phys. Fluids **31**, 087103 (2019).

[63] Mohan, L., R. T. Bonnecaze, and M. Cloitre, "Microscopic origin of internal stresses in jammed soft particle suspensions," Phys. Rev. Lett. **111**, 268301 (2013).

[64] Mohan, L., M. Cloitre, and R. T. Bonnecaze, "Build-up and two-step relaxation of internal stress in jammed suspensions," J. Rheol. **59**, 63–84 (2015).

[65] Osuji, C. O., C. Kim, and D. A. Weitz, "Shear thickening and scaling of the elastic modulus in a fractal colloidal system with attractive interactions," Phys. Rev. E **77**, 060402 (2008).

[66] Negi, A. S., and C. O. Osuji, "New insights on fumed colloidal rheology—Shear thickening and vorticity-aligned structures in flocculating dispersions," Rheol. Acta **48**, 871–881 (2009).

[67] Negi, A. S., and C. O. Osuji, "Physical aging and relaxation of residual stresses in a colloidal glass following flow cessation," J. Rheol. **54**, 943–958 (2010).

[68] Moller, P., A. Fall, V. Chikkadi, D. Derks, and D. Bonn, "An attempt to categorize yield stress fluid behaviour," Philos. Trans. Ser. A: Math. Phys. Eng. Sci. **367**, 5139–5155 (2009).

[69] Cheng, X., J. H. McCoy, J. N. Israelachvili, and I. Cohen, "Imaging the microscopic structure of shear thinning and thickening colloidal suspensions," Science **333**, 1276–1279 (2011).

[70] Wagner, N. J., and J. F. Brady, "Shear thickening in colloidal dispersions," Phys. Today **62** (10), 27–32 (2009).

[71] Ballesta, P., R. Besseling, L. Isa, G. Petekidis, and W. C. K. Poon, "Slip and flow of glassy hard sphere colloidal suspensions," Phys. Rev. Lett. **101**, 258301 (2008).

[72] Ballesta, P., G. Petekidis, L. Isa, W. C. K. Poon, and R. Besseling, "Wall slip and flow of concentrated hard-sphere colloidal suspensions," J. Rheol. **56**, 1005–1037 (2012).

[73] Meeker, S. P., R. T. Bonnecaze, and M. Cloitre, "Slip and flow in soft particle pastes," Phys. Rev. Lett. **92**, 198302 (2004).

[74] Läuger, J., and H. Stettin, "Effects of instrument and fluid inertia in oscillatory shear in rotational rheometers," J. Rheol. **60**, 393–406 (2016).

[75] Schrag, J. L., "Deviation of velocity gradient profiles from the 'gap loading' and 'surface loading' limits in dynamic simple shear experiments," Trans. Soc. Rheol. **21**, 399–413 (1977).

[76] Krieger, I. M., "Bingham award lecture—1989: The role of instrument inertia in controlled-stress rheometers," J. Rheol. **34**, 471–483 (1990).

[77] Athanasiou, T., G. K. Auernhammer, D. Vlassopoulos, and G. Petekidis, "A high-frequency piezoelectric rheometer with validation of the loss angle measuring loop: Application to polymer melts and colloidal glasses," Rheol. Acta **58**, 619–637 (2019).

[78] Laurati, M., G. Petekidis, N. Koumakis, F. Cardinaux, A. B. Schofield, J. M. Brader, M. Fuchs, and S. U. Egelhaaf, "Structure, dynamics, and rheology of colloid-polymer mixtures: From liquids to gels," J. Chem. Phys. **130**, 134907 (2009).

[79] Carrier, V., and G. Petekidis, "Nonlinear rheology of colloidal glasses of soft thermosensitive microgel particles," J. Rheol. **53**, 245–273 (2009).

[80] Paulin, S. E., B. J. Ackerson, and M. S. Wolfe, "Equilibrium and shear induced nonequilibrium phase behavior of PMMA microgel spheres," J. Colloid Interface Sci. **178**, 251–262 (1996).

[81] Laurati, M., P. Maßhoff, K. J. Mutch, S. U. Egelhaaf, and A. Zaccone, "Long-lived neighbors determine the rheological response of glasses," Phys. Rev. Lett. **118**, 018002 (2017).

[82] Sollich, P., "Rheological constitutive equation for a model of soft glassy materials," Phys. Rev. E **58**, 738–759 (1998).

[83] Miyazaki, K., H. M. Wyss, D. A. Weitz, and D. R. Reichman, "Nonlinear viscoelasticity of metastable complex fluids," Europhys. Lett. **75**, 915–921 (2006).

[84] Derec, C., G. Ducouret, A. Ajdari, and F. Lequeux, "Aging and nonlinear rheology in suspensions of polyethylene oxide-protected silica particles," Phys. Rev. E **67**, 061403 (2003).